Modeling of Modulation Formats for Interferometric Noise Mitigation

Giuseppe Talli, *Member, IEEE*, Chi Wai Chow, *Member, IEEE*, and Paul D. Townsend, *Member, IEEE*

***Abstract*—Interferometric noise in optical communication systems employing reflective modulation schemes can be mitigated by reshaping the data spectrum to reduce the spectral overlap with backscattered and backreflected light. A novel analytical model, capable of analyzing accurately the performance of modulation formats with a wide optical spectrum, is derived here and applied to study the case of interferometric noise caused by Rayleigh backscattering. Compared to more complex models and simulations the new method is fast, simple to implement, and gives clear insight into the physical phenomena involved. In addition, the performance of practical systems can be easily analyzed and optimized due to the capability of the model to include real component specifications such as arbitrary optical and electrical filter responses. The specific case of phase-modulated non-return to zero (PM-NRZ) modulation format is used to validate the model against experimental results and excellent agreement is obtained. The PM-NRZ performance is also investigated as a function of various parameters, quantifying, for example, the trade-off between phase modulation index and interferometric noise mitigation.**

***Index Terms*—Interferometric noise, modeling, modulation formats, optically preamplified receiver, passive optical network (PON), phase modulation, Rayleigh backscattering (RB).**

I. Introduction

PASSIVE optical networks (PONs) are highly attractive optical access architectures because of the shared infrastructure and the absence of active routing components in the path between the head-end office and the customer [1]. The introduction of dense wavelength division multiplexing (DWDM) offers a potentially cost effective way of increasing the bandwidth or the number of customers supported in these architectures through increased use of the wavelength domain [2]–[4]. Reflective modulators (R-Mods), operated in conjunction with the optical carrier provided by a centralized light source (CLS), are a promising solution to deploy a cost effective, high bit rate (10 Gbit/s or above) wavelength independent transmitters in these architectures [5], [6]. However, since the optical carrier and modulated upstream signal share the same path, this scheme may suffer from interferometric noise caused by localized Fresnel back-reflections [6] and Rayleigh backscattering (RB) [7].

A range of techniques employing advanced modulation formats have recently been the subject of increasing interest due to their effectiveness at mitigating the interferometric noise by reducing the spectral overlap between signal and interferer [8]–[10]. As an example, the phase-modulated non-return-to-zero (PM-NRZ) modulation scheme has been shown to be effective in the presence of high levels of backscattering and back-reflections [8], [11]. This technique has also been experimentally tested in a hybrid DWDM time-division-multiplexing (TDM), 116 km reach, PON capable of supporting a split ratio of 256 in each TDM PON [12]. However, in order to optimize a network design employing this type of technique, it is necessary to efficiently model the effectiveness of the noise mitigation scheme as a function of the power of the interferers, RB or localized reflections.

Modeling the performance of this type of mitigation scheme is challenging due to the large optical spectrum of the upstream signal. The interaction of these schemes with an optically preamplified receiver is particularly important due to the narrow optical filters commonly used and the additional presence of amplified spontaneous emission (ASE). The usual approximation methods employed to model systems in the presence of ASE [13], [14] would provide inaccurate results because, firstly, the spectrum of the interfering signal cannot be considered white, and secondly, the spectrum of the modulated signal is wider than the optical filter bandwidth. Numerical simulations and time domain models [15]–[17] could be employed to obtain accurate results, but they would generally provide limited physical insight and also be relatively demanding from a computational point of view, thus limiting their effectiveness in the optimization of the overall system performance.

Therefore, the objective of this paper is to derive a novel modeling approach that can be easily implemented and used efficiently to study the performance of noise mitigation schemes employing arbitrary modulation formats. The theoretical analysis presented here is focused on the interferometric noise generated by RB, although it could be extended to other sources of interferometric noise. The case of an optically preamplified receiver is modeled with sufficient flexibility to include arbitrary optical and electrical filter responses. The various noise contributions are derived from the power spectral densities (PSDs) of the optical signals and the performance of the scheme is

Manuscript received November 28, 2007; revised April 29, 2008. Current version published December 19, 2008. This work was supported in part by the Science Foundation Ireland under Grant 03/IN1/1340 and Grant 06/IN/I969 and in part by the European Commission under project PIEMAN.

G. Talli and P. D. Townsend are with the Photonic Systems Group, Tyndall National Institute and Department of Physics, University College Cork, Cork, Ireland (e-mail: giuseppe.talli@tyndall.ie; paul.townsend@tyndall.ie).

C. W. Chow is with the Photonic Systems Group, Tyndall National Institute and Department of Physics, University College Cork, Cork, Ireland, and also with the Department of Photonics, National Chiao Tung University, Hsinchu, Taiwan, R.O.C. (e-mail: cwchow@faculty.nctu.edu.tw).

Color versions of one or more of the figures in this paper are available online at http://ieeexplore.ieee.org.

Digital Object Identifier 10.1109/JLT.2008.926922

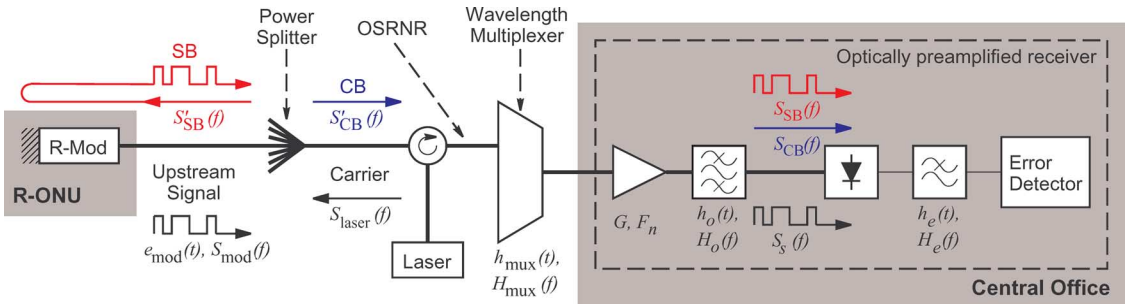

Fig. 1. Schematic of the upstream signal direction in a DWDM-PON employing CLS.

then modeled analytically. This allows a rapid evaluation of the various parameters and choice of components, such as, for example, the modulator characteristics, receiver frequency response, optical filter shape and detuning. Moreover, in contrast to simulations or more complex models, this approach provides an immediate insight into the physical phenomena that determine the performance of the noise mitigation scheme.

The next section presents a brief description of a DWDM-PON architecture employing CLS and describes the sources of RB in this architecture. The model of the RB interferometric noise is derived in Section III, while the model of the optically preamplified receiver is described in Section IV. The PM-NRZ mitigation scheme is then briefly reviewed in Section V and is then used to verify the model in Section VI. Modeling results are compared with experiments performed using two optical receivers with different frequency responses. The model is also used to analyze the noise suppression introduced by the PM-NRZ scheme as a function of the optical filter detuning and the phase modulation index.

II. Centralized Light Source PON

Fig. 1 illustrates schematically the upstream of a DWDM-PON employing CLS. The optical carrier generated in a remote location is delivered to the customer reflective optical networking unit (R-ONU) through the access link, which, apart from fibers, can also include power splitters if TDM is used to share the network capacity. The carrier is modulated in the R-Mod and transmitted back towards the receiver in the central office, which is represented in the figure by an optically preamplified receiver. Wavelength multiplexers and demultiplexers are present in the system in order to concentrate the various DWDM channels for transmission towards the central office and then to divide the channels before the receivers. The location of these components within the network depends on the specific architecture employed [3], [6]. In Fig. 1, the multiplexer is located after the carrier injection, as it would be in a long-reach architecture [3], and the demultiplexer is the optical filter located within the optically preamplified receiver.

When a single fiber is used to transmit the optical carrier and the upstream signal, localized Fresnel back-reflections and RB are the cause of interferometric noise. RB, however, differs from localized back-reflections due to its distributed nature. In particular, the intensity of RB generated from high-speed modulated light is time independent due to the averaging effect along the spatial extent of the fiber [7], in contrast to the localized back-reflection case where the reflected light remains modulated. In addition, RB from polarized light is only partially polarized. Moreover, while the level of back-reflection in an optical system can, in principle, be controlled by setting appropriate return loss specifications for the various optical components, the RB is an intrinsic phenomenon in fiber propagation and its level is determined by the fiber type and configuration used.

In these architectures, there are two RB contributions, which interfere with the upstream signal at the receiver. As shown in Fig. 1, the first contribution, carrier backscattering (CB), arises from the continuous wave carrier delivered to the customer. The second contribution, signal backscattering (SB), is generated by the modulated upstream signal. The backscattered light re-enters the R-ONU where it is re-modulated and reflected towards the receiver. This relatively low power light is also amplified by the R-Mod, which is usually arranged to provide net gain in order to overcome the loss introduced by the carrier delivery path. The relative strengths of the two noise contributions depend on the reflective modulator gain, fiber lengths, and distribution of the splitters [6], [12].

III. Rayleigh Backscattering Interferometric Noise

An accurate theoretical derivation of the properties of RB and the interferometric noise that it generates can be found in [7]. The final results, however, are derived under the assumption that the modulation spectrum is smaller than the laser linewidth, which is valid only for restricted cases, such as very low bit rate systems. In contrast, in current systems with high bit rates of 10 Gbit/s and above and for the spectrally broadened scheme analyzed here, this assumption no longer holds true. The actual spectrum of the high-speed modulated signal needs to be considered in order to obtain an accurate prediction of the system performance and a more general derivation should also account for RB with a spectrum wider than the data signal. The latter case is representative of the SB, where the backscattered light from a modulated signal is re-modulated, thus further broadening the spectrum.

Following the notation introduced in [7], the complex amplitude of the electrical field at the output of the modulator is given by

$$e_{\mathrm{mod}} = \sqrt{P_0}\gamma(t)e^{j\phi(t)} \tag{1}$$

where $\sqrt{P_0}$ is the field amplitude normalized such that its squared magnitude is equal to the optical power,

$\gamma(t) = \sqrt{a(t)}\exp[j\theta(t)]$ represents the variation of the complex amplitude due to amplitude or phase modulation and $\phi(t)$ describes the laser phase noise. In general, $\gamma(t)$ is nonstationary, and, thus, the complex modulated signal amplitude $e_{\mathrm{mod}}(t)$ is also a nonstationary random process. However, considering digital modulation, $e_{\mathrm{mod}}(t)$ is found to be a cyclostationary process. The electric field PSD of the signal at the output of the modulator, $S_{\mathrm{mod}}(f)$, is, thus, given by the Fourier transform of the time averaged autocorrelation function, which is periodic with period equal to the symbol duration of the modulating signal. Similarly it is possible to define the PSD of the backscattered light electric field, $S'_b(f)$, where the subscript $_b$ identifies the backscattering contribution, either CB or SB. Since the CB is generated by the backscattering of the carrier its PSD is the same as that of the laser, $S_{\mathrm{laser}}(f)$ [7], while the SB PSD, $S'_{\mathrm{SB}}(f)$, can be evaluated as the convolution of the PSDs of the modulated optical signal and the modulation signal. The PSD of the upstream signal, $S_s(f)$, and backscattering, $S_b(f)$, after reshaping by the wavelength multiplexers and the optical filter inside the receiver (Fig. 1) can thus be simply derived as

$$S_s(f)=G' S_{\mathrm{mod}}(f)\cdot\left|H_{\mathrm{mux}}(f+\nu_0)\right|^2\cdot\left|H_o(f+\nu_0)\right|^2 \quad (2)$$

$$S_b(f)=G' S'_b(f)\cdot\left|H_{\mathrm{mux}}(f+\nu_0)\right|^2\cdot\left|H_o(f+\nu_0)\right|^2 \quad (3)$$

where ν_0 is the laser center frequency, H_{mux} and H_o are, respectively, the frequency response of the wavelength multiplexers/demultiplexers and of the receiver optical filter, normalized such that $H_{\mathrm{mux}}(\nu_0) = H_o(\nu_0) = 1$. G' is the net gain that includes both the amplifier gain G and the insertion loss of the optical filters.

The PSD of the photocurrent, $S_{I_t}(f)$, can then be derived as in [7] from $S_s(f)$ and $S_b(f)$. Assuming that within the observation interval there are no changes in the signal and RB powers due to modulation, the variance of the interferometric noise can thus be evaluated, after being detected and filtered by the photodetector frequency response, as

$$\sigma^2_{i_t} = \mathcal{D}^2\int_{-\infty}^{+\infty}\left|H_e(f)\right|^2\left\{k\left[S_s(f)*S_b(f)+S_b(f)*S_s(f)+\frac{1+p^2}{2}S_b(f)*S_b(f)\right]\right\}df \quad (4)$$

where $*$ denotes deterministic cross-correlation, $\mathcal{D}$ is the photodetector responsivity, $H_e(f)$ is the electrical filter normalized frequency response, such that $H_e(0) = 1$, and k and p are polarization coefficients, with $p = 2k - 1$. The polarization coefficient k equals 1 for completely polarized backscattering $(p = 1)$ aligned with the signal polarization, and $k = 0.5$ for a completely depolarized backscattered field $(p = 0)$. In practice, roughly 1/3 of the RB light is polarized, giving $p \approx 0.556$, and $k \approx 0.667$ and $k \approx 0.333$, respectively, for a signal co- and cross-polarized with respect to the backscattered light [7], [18]. In the remainder of this paper, only the co-polarized case is considered, which corresponds to the highest noise and, hence , worst case.

In practice, it is useful to separate the two terms inside the integral in (4). By analogy with the noise generated by spontaneous emission, the first term can be identified as the noise created by the beating of the signal and RB

$$\sigma^2_{s,b} = \mathcal{D}^2\int_{-\infty}^{+\infty}\left|H_e(f)\right|^2 k\left[S_s(f)*S_b(f)+S_b(f)*S_s(f)\right]df = \beta_{s,b}2k\mathcal{D}^2P_sP_b \quad (5)$$

where P_s and P_b are the total mean powers of the signal and backscattered light respectively, and $\beta_{s,b}$ is defined as

$$\beta_{s,b} = \frac{1}{2}\int_{-\infty}^{+\infty}\left|H_e(f)\right|^2 k\left[s_s(f)*s_b(f)+s_b(f)*s_s(f)\right]df \quad (6)$$

with $s_s(f)$ and $s_b(f)$ the normalized spectra of, respectively, signal and backscattering defined as

$$s_s(f) = \frac{S_s(f)}{P_s} = \frac{S_s(f)}{\int_{-\infty}^{+\infty}S_s(f)df} \quad (7)$$

$$s_b(f) = \frac{S_b(f)}{P_b} = \frac{S_b(f)}{\int_{-\infty}^{+\infty}S_b(f)df}. \quad (8)$$

On the other hand, the second term of (4) represents the noise generated by the RB beating with itself

$$\sigma^2_{b,b} = \mathcal{D}^2\int_{-\infty}^{+\infty}\left|H_e(f)\right|^2\frac{1+p^2}{2}S_b(f)*S_b(f)df = \beta_{b,b}\frac{1+p^2}{2}\mathcal{D}^2P_b^2 \quad (9)$$

where $\beta_{b,b}$ is defined as

$$\beta_{b,b} = \int_{-\infty}^{+\infty}\left|H_e(f)\right|^2 s_b(f)*s_b(f)df. \quad (10)$$

For low levels of RB, this second component is small compared to the first one, and can thus be neglected in the analysis of modulation formats that are highly sensitive to RB noise such as, for example, NRZ [18]. However, the contribution of the second component is non-negligible for higher RB levels that are present, for example, in schemes with an increased immunity to RB noise.

An important advantage of using cyclostationary PSDs is that the noise variances are time independent, and, therefore, they account for the noise of all the symbols in a sequence. In contrast, adopting a time domain approach similar to [15]–[17] would require the calculation of an explicit average of the error probability and further optimization of the decision threshold and sampling point over the entire bit sequence.

Different modulation formats are expected to produce distinct values for $\beta_{s,b}$ and $\beta_{b,b}$ due to the effect of the optical and electrical filtering on the different PSDs. The noise due to SB is also expected to differ from that due to CB, because in the former case the backscattered light is doubly modulated and, thus, spectrally broadened. The SB is also synchronously modulated with

the signal, and, thus, the SB power for a 0 and a 1 can be calculated in the case of NRZ power modulation as

$$P_{\mathrm{SB}|0} = \overline{P_{\mathrm{SB}}}\frac{2}{m+1} \tag{11}$$

$$P_{\mathrm{SB}|1} = \overline{P_{\mathrm{SB}}}\frac{2m}{m+1} \tag{12}$$

where the extinction ratio is given by m and $\overline{P_{\mathrm{SB}}}$ is the average SB power.

IV. Optically Preamplified Receiver

Assuming Gaussian statistics for the noise and optimal decision threshold, the BER can be modeled as

$$\mathrm{BER} = \frac{1}{2}\mathrm{erfc}\left(\frac{Q}{\sqrt{2}}\right) \tag{13}$$

where $\mathrm{erfc}(\cdot)$ is the complementary error function defined as

$$\mathrm{erfc}(x) = \frac{2}{\sqrt{\pi}}\int_x^\infty \exp(-w^2)dw. \tag{14}$$

The Q factor is defined as

$$Q = \frac{I_1 - I_0}{\sigma_1 + \sigma_0} \tag{15}$$

where I_1 and I_0 are the photocurrents for the 1 s and the 0 s, respectively. The assunption of Gaussian statistics is widely used in the case of ASE noise as it enables simple, relatively accurate calculations to be performed [16]. Similarly, in the case of RB, the assumption of Gaussian statistics has been shown experimentally to lead to accurate noise estimates [7].

The total noise on the bits 0 and 1 can be separated into thermal, shot, signal-ASE beat and ASE-ASE beat noise as [13], [14], plus the contributions from the RB beat noise

$$\sigma_x^2 = \sigma_{\mathrm{therm}}^2 + \sigma_{\mathrm{shot}|x}^2 + \sigma_{s,\mathrm{ASE}|x}^2 + \sigma_{\mathrm{ASE,ASE}}^2 + \sigma_{\mathrm{RB}|x}^2 \tag{16}$$

where the subscript $_x$ indicates the dependence on the data symbol, either 0 or 1, and σ_{therm} is the receiver thermal noise. The shot noise can be derived as

$$\sigma_{\mathrm{shot}|x}^2 = 2q\mathcal{D}(P_{s|x} + P_{\mathrm{ASE}} + P_{\mathrm{CB}} + P_{\mathrm{SB}|x})B_e \tag{17}$$

where q is the electron charge and B_e is the equivalent bandwidth of the electrical filter. The power of the ASE, P_{ASE}, can be derived from the integral of the power spectral density of the ASE at the receiver, $S_{\mathrm{ASE}}(f)$

$$P_{\mathrm{ASE}} = 2\int_0^{+\infty} S_{\mathrm{ASE}}(f)df = 2S_{\mathrm{EDFA}}B_{\mathrm{o}} \tag{18}$$

where the factor 2 accounts for the two polarizations of the ASE, S_{EDFA}, is the power spectral density of the ASE at the output of the EDFA and B_{o} is the equivalent bandwidth of the optical filter defined as

$$B_o = \int_0^{+\infty} |H_o(f)|^2\, df. \tag{19}$$

S_{EDFA} can, to a first approximation, be considered independent of frequency, since its bandwidth is much broader than the optical filters employed, and can be derived from the gain, G and noise figure F_n of the amplifier [14]

$$S_{\mathrm{EDFA}} \simeq \frac{1}{2}F_nGh\nu_0 \tag{20}$$

where h is the Plank constant.

Under the same assumption used to derive the RB noise, the variance of the signal-ASE beat noise is

$$\sigma_{s,\mathrm{ASE}|x}^2 = \mathcal{D}^2\int_{-\infty}^{+\infty} |H_e(f)|^2 \left[S_{s|x}(f) * S_{\mathrm{ASE}}(f) + S_{\mathrm{ASE}}(f) * S_{s|x}(f)\right] df. \tag{21}$$

By analogy with [13] and [14], the previous equation can be rewritten as

$$\sigma_{s,\mathrm{ASE}|x}^2 = 4\mathcal{D}^2P_{s|x}S_{\mathrm{EDFA}}B_{s,\mathrm{ASE}} \tag{22}$$

where we define $B_{s,\mathrm{ASE}}$ as the equivalent receiver bandwidth for this noise contribution, given by

$$B_{s,\mathrm{ASE}} = \frac{1}{4}\int_{-\infty}^{+\infty} |H_e(f)|^2 \Big[s_s(f) * |H_o(f+\nu_0)|^2 + |H_o(f+\nu_0)|^2 * s_s(f)\Big] df. \tag{23}$$

Following the same derivation as in [19], but with slightly different notation, the noise contribution due to the ASE-ASE beat noise can be calculated as

$$\sigma_{\mathrm{ASE,ASE}}^2 = 4\mathcal{D}^2S_{\mathrm{EDFA}}^2B_oB_{\mathrm{ASE,ASE}} \tag{24}$$

where $B_{\mathrm{ASE,ASE}}$ is the equivalent bandwidth of this noise component defined as

$$B_{\mathrm{ASE,ASE}} = \frac{1}{2B_o}\int_{-\infty}^{+\infty} |H_e(f)|^2 \times \Big[|H_o(f+\nu_0)|^2 * |H_o(f+\nu_0)|^2\Big] df. \tag{25}$$

Using the notation introduced in the previous sections, the contributions from the RB beat noise are calculated as

$$\sigma_{\mathrm{RB}|x}^2 = \sum_b(\sigma_{s,b|x}^2 + \sigma_{\mathrm{b,b}|x}^2 + \sigma_{b,\mathrm{ASE}|x}^2) \tag{26}$$

where, as in the previous section, the subscript $_b$ indicates either CB or SB. The variance of the noise generated by the ASE beating with the CB or SB, $\sigma_{b,\mathrm{ASE}|x}$, can simply be evaluated as

$$\sigma_{\mathrm{b,ASE}|x}^2 = 4\mathcal{D}^2P_{\mathrm{b}|x}S_{\mathrm{EDFA}}B_{\mathrm{b,ASE}} \tag{27}$$

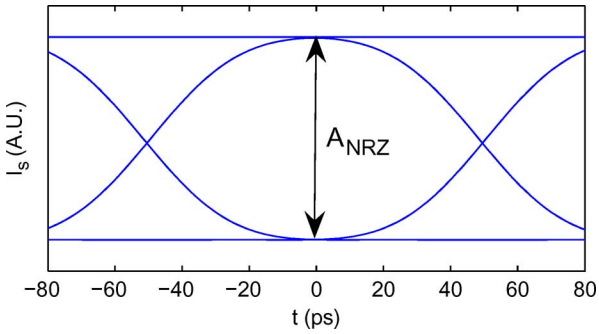

Fig. 2. Example of a modelled eye-diagram for 10-Gbit/s NRZ modulation format.

where, by analogy with the signal-ASE beat case, the equivalent bandwidth of the backscattering-ASE noise can be defined as

$$B_{b,\mathrm{ASE}} = \frac{1}{4}\int_{-\infty}^{+\infty} |H_e(f)|^2 \left[s_b(f) * |H_o(f+\nu_0)|^2 + |H_o(f+\nu_0)|^2 * s_b(f) \right] df. \quad (28)$$

The effect of both optical and electrical filters on the pulse shape of the photo-detected current, and hence on the levels I_1 and I_0, can be modeled by analyzing an eye-diagram in the absence of noise. The signal photocurrent can be derived by convolving the signal power after propagation through the optical filters and amplifiers, $P_s(t)$, with the impulse response of the electrical filter $h_e(t)$, to obtain

$$\begin{aligned} I_s(t) &= \mathcal{D} P_s \otimes h_e(t) \\ &= \mathcal{D} G' \left| e_{\mathrm{mod}} \otimes (h_{\mathrm{mux}} \otimes h_{\mathrm{o}})(t) \right|^2 \otimes h_e(t) \end{aligned} \quad (29)$$

where $\otimes$ indicates convolution, and $P_s(t)$ is obtained by convolving the electric field of the upstream signal at the output of the modulator with the low-pass equivalent impulse response of the optical filters, $h_{\mathrm{mux}}(t)$ and $h_{\mathrm{o}}(t)$. The opening of the eye-diagram depends both on the modulation format used and on the optical and electrical filters. As an example, Fig. 2 presents an eye diagram for an NRZ modulation format with eye opening, A_{NRZ}, defined as the difference between the average levels for 0 s and 1 s normalized to the average signal power, $\overline{P_s}$.

Following a similar method to that proposed in [19], we approximate the photocurrent level at the sampling point for 0 s and 1 s as

$$I_0 = \mathcal{D} P_{s|0} = \eta_{\mathrm{eye}} \mathcal{D} \overline{P_s} \frac{2}{m+1} \quad (30)$$

$$I_1 = \mathcal{D} P_{s|1} = \eta_{\mathrm{eye}} \mathcal{D} \overline{P_s} \frac{2m}{m+1} \quad (31)$$

where $P_{s|0}$ and $P_{s|1}$ are respectively the signal power of the 0 s and the 1 s, and m is the extinction ratio. Since the shape of the eye-diagram can differ from the NRZ case, as shown in Section VI, the parameter η_{eye} accounts for the eye opening ratio compared to an idealized NRZ modulation case, and is defined as $\eta_{\mathrm{eye}} = A_{\mathrm{eye}}/A_{\mathrm{NRZ}}$.

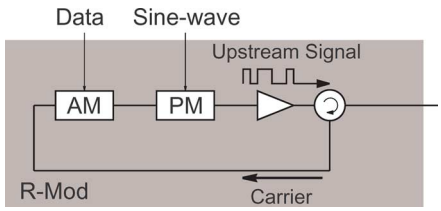

Fig. 3. Structure of the reflective modulator generating PM-NRZ upstream signal.

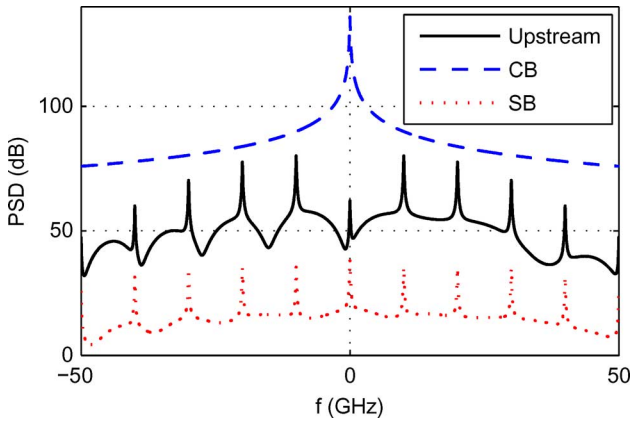

Fig. 4. PSDs of the PM-NRZ upstream signal and of the two corresponding RB components.

V. Phase Modulated Non-return to Zero

The PM-NRZ modulation scheme, due to its wide spectrum, serves as a good example to validate the model described in the previous sections. In order to reduce the spectral overlap between the data signal and the backscattering, the PM-NRZ modulation format uses a phase modulator purposely overdriven to generate multiple side-bands and to suppress the center wavelength [8], [11]. The PM-NRZ signal can be generated using a R-Mod with the structure outlined in Fig. 3. This comprises a circulator, an amplitude modulator, which provides the NRZ data modulation, a phase modulator driven with a sinusoid synchronized with and at the frequency of the NRZ data, and an optical amplifier that can be used to boost the power at the output of the R-Mod. The phase modulation index, and, hence, the drive voltage of the phase modulator is set so as to obtain the desired suppression of the center wavelength. Fig. 4 presents, as an example, the PSDs modeled for upstream signal, CB and SB with an NRZ data rate of 10 Gbit/s and with the phase modulator driven with a 10-GHz sinusoid, where, for clarity, the spectra are presented in arbitrary units. The differences between the spectra are evident, and in particular we note the wider spectrum of the SB caused by the double PM-NRZ modulation. The asymmetry in the signal PSD is caused by the phase alignment between NRZ and sine modulation optimized to obtain the highest eye opening [11].

The effectiveness of the PM-NRZ modulation format against the RB noise can be increased by using optical filters to selectively attenuate the RB by a greater amount than the upstream signal. As an example, in [8], the use of a specifically tailored narrow notch filter, with 3 dB width equal to ∼0.05 nm, is proposed to reduce the optical power of the CB compared to

TABLE I
RECEIVER PARAMETERS

	Rx 1	Rx 2
G'	19 dB	21 dB
F_n	5 dB	4 dB
H_o	Gaussian	Gaussian
$B_{H_o\|3\text{dB}}$	50 GHz	50 GHz
$\mathcal{D}$	1.25 A/W	1.25 A/W
σ_{th}	4 μA	2 μA
$H_{e,1}, H_{e,2}$	Bessel-Thomson 4th order	Bessel-Thomson 4th order
$B_{H_{e,1}\|3\text{dB}}$	8 GHz	9 GHz
$B_{H_{e,2}\|3\text{dB}}$	-	7.5 GHz

the signal. A simpler alternative, recently demonstrated by our group [11], uses offset channel tuning to achieve the required optical filtering effects from the wavelength multiplexers/demultiplexers already present in a DWDM PON, for example arrayed-waveguide-gratings (AWGs), in place of additional notch filters. Another beneficial effect of the detuned filtering is the reduction of the overall spectral-width of the upstream signal, which increases the chromatic dispersion tolerance to more 340 ps/nm, which corresponds to ~20 km of standard single mode fiber [11]. Depending on the exact architectural configuration, the detuning of the multiplexers in the upstream path must be selected in order to minimize the loss in the carrier delivery path. In the example of a long-reach hybrid DWDM-TDM PON, both upstream AWGs can be detuned without introducing extra loss [12].

VI. RESULTS AND DISCUSSION

In order to highlight the capabilities of the model, this section presents a comparison between modeling and experimental results for the PM-NRZ modulation scheme using two different optically preamplified receivers with the parameters shown in Table I. The frequency response of the electrical filter in the first receiver, Rx 1, is approximated by a Bessel-Thomson filter of 4th order with 3-dB bandwidth of 8 GHz, while in the second receiver, Rx 2, it is approximated by a series of two 4th order Bessel-Thomson filters with 3-dB bandwidth of 9 and 7.5 GHz, respectively. The practical realization of Rx 2 is a combination of an optical receiver module and a separate filter, which results in a sharper filtering. The optical filter within the receiver and the wavelength multiplexer are both Gaussian AWGs, with 3-dB bandwidth of 50 GHz, and are tuned to the same wavelength.

Analytical expressions can be used to represent the various PSDs as in [18] and to derive the various noise contributions. However, the analytical description of the spectrum of the PM-NRZ modulation is relatively complex, and, thus, here we simply derived the various PSDs required in the model from the numerical Fourier transform of $e_{\text{mod}}(t)$ for a 10 Gbit/s $2^{11}-1$ pseudo-random bit sequence (PRBS). As an example, the PSDs shown in Fig. 4 are obtained for PM-NRZ with an NRZ extinction ratio of 12 dB and a PM index of 2.28, which corresponds to 18 dB suppression of the carrier power. The numerical evaluation of $e_{\text{mod}}(t)$ is also advantageous since it provides a simple way to calculate the shape of the received pulses and thus the eye opening ratio, η_{eye}.

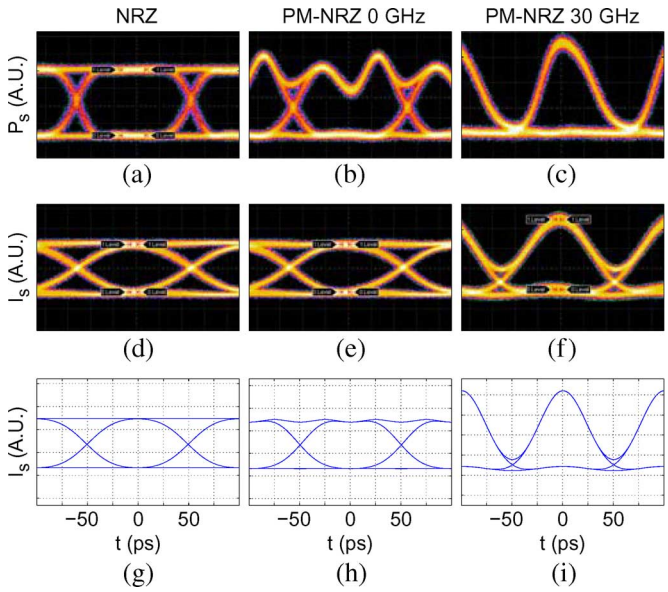

Fig. 5. Experimental optical (a)–(c) and electrical (d)–(f) eye-diagrams for NRZ and PM-NRZ at different detunings compared to the corresponding modeled electrical eye-diagrams (g)–(i).

Fig. 5 shows typical optical eye-diagrams (amplitudes not to scale), obtained experimentally for 10 Gbit/s signals with a 30-GHz photodetector, for: (a) NRZ modulation format, with both AWGs tuned to the laser frequency; (b) PM-NRZ, with both AWGs tuned to the laser frequency; and (c) PM-NRZ with the AWGs detuned by 30 GHz. It is interesting to note in Fig. 4 (b) the shape of the eye diagram for PM-NRZ with no detuning, where two peaks appear, corresponding to a 20-GHz sine wave, which results from the beating of the sidebands at ± 10 GHz. Conversely, when the optical filters are detuned, as in Fig. 5(c), the strongest beating is between the components at $+10$ and $+20$ GHz, which produces the return-to-zero (RZ) appearance of the signal due to 10-GHz sine modulation.

Fig. 5(d)–(f) shows the electrical eye-diagrams obtained from Rx 1, where the effect of the electrical filter can clearly be seen in the increased rise and fall times of the NRZ signal and in the cancellation of the 20-GHz component for the nondetuned PM-NRZ. However, in the case of the 30-GHz-detuned PM-NRZ, the frequency response of the electrical filter is not sharp enough to strongly affect the 10-GHz component, which is only slightly attenuated, resulting in an eye-diagram that again has an RZ appearance, as shown in Fig. 5(f).

Equation (29) can be used to model the eye-diagrams in the various cases, starting from $e_{\text{mod}}(t)$. The results, using Rx 1 filter characteristic, can be seen in Fig. 5(g)–(i), respectively, for NRZ and PM-NRZ with 0 and 30 GHz detuning. The excellent agreement in shape between the modeled and experimental eye-diagrams is a first indication that the model can describe accurately the received PM-NRZ signal.

The qualitative agreement shown by the eye diagrams is also supported quantitatively by measurements of the receiver sensitivity. The sensitivity of the optically preamplified receiver for PM-NRZ modulation varies as a function of the optical filter detuning due to its wide spectrum and complex pulse shape [11].

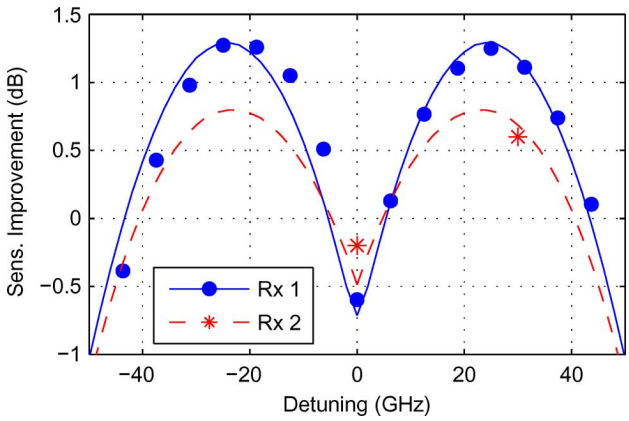

Fig. 6. Measured (symbols) and modeled (lines) improvement of the receiver sensitivity for PM-NRZ modulation as a function of the detuning for Rx 1 and Rx 2 compared to NRZ with no detuning.

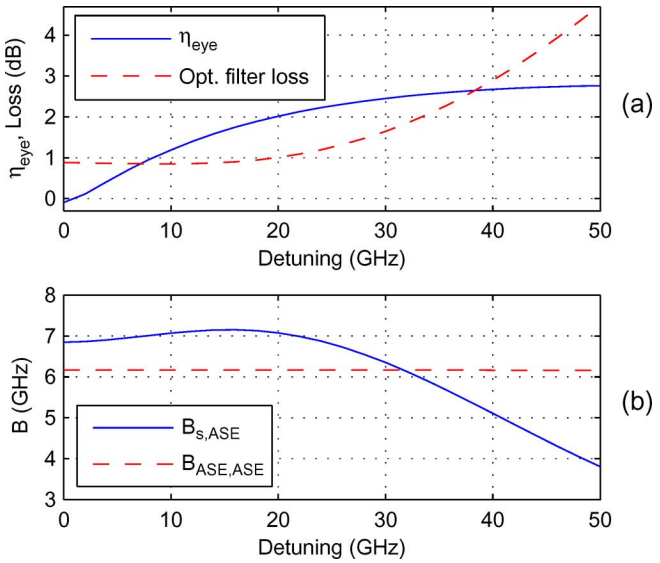

Fig. 7. Loss in the receiver optical filter compared to the eye opening improvement (a) and equivalent noise bandwidths (b) as a function of the filter detuning for Rx 1.

The symbols in Fig. 6 present an accurate experimental characterization of the sensitivity of the optically preamplified receiver Rx 1 as a function of the detuning for the PM-NRZ scheme. The results show that the sensitivity improvement, defined as the difference between the PM-NRZ and the NRZ sensitivity with no detuning, displays two maxima for detuning of around ± 25 GHz. We also note a slight asymmetry of the two maxima which is caused by a slight distortion in the electrical sinusoidal signal used to drive the PM, with an asymmetry in rise and fall times [11].

The sensitivity improvement derived from the optically preamplified receiver model for Rx 1 is also compared with the experiments in Fig. 6, showing excellent agreement and proving the ability of the model to accurately predict the performance of complex modulation formats. Since the model is essentially analytical, it offers the advantage of providing, in a simple way, insights into the physical phenomena that govern the sensitivity for the PM-NRZ scheme. Fig. 7(a) presents the eye-opening factor, η_{eye}, and the loss introduced inside the receiver by the detuning of the optical filter. The latter, however, should not be confused with the insertion loss at the center frequency of the filter which is already included in the net gain G'.

These two factors have opposite effects, with η_{eye} causing an improvement in sensitivity with increased detuning due to the RZ-like shape of the eye, while the filter loss reduces the actual optical power reaching the photodetector causing a reduction of the overall receiver sensitivity. We note that the difference between the two corresponds roughly to the sensitivity improvement in Fig. 6, with a small difference that can be attributed, for example, to the change with the detuning of the equivalent noise bandwidth, $B_{\mathrm{s,ASE}}$. This third effect, which can be seen in Fig. 7(b), has a smaller influence on the sensitivity, but it is noteworthy that the value of the equivalent bandwidths $B_{\mathrm{s,ASE}}$ and $B_{\mathrm{ASE,ASE}}$ are substantially lower than that commonly used due to the wide spectrum of the signal.

Fig. 6 also presents the comparison between modeled and experimental sensitivity improvement in the case of receiver Rx 2, which is the receiver used in the experimental characterization reported in [11]. Although there are only two experimental points, good agreement is also observed. In this case the sensitivity improvement caused by the detuning is smaller compared to Rx 1 due to the sharper electrical filtering that reduces the eye-opening increase. Although not shown here, experimental and modeled eye-diagrams are in good agreement, with a shape close to NRZ for all detuning.

The performance of the PM-NRZ scheme against the RB noise can be quantified by the receiver power penalties at a bit error rate (BER) of 10^{-9} as a function of the optical-signal-to-Rayleigh-noise ratio (OSRNR). However, the direct characterization in a PON is difficult since the polarization state cannot be accurately controlled and the SB power cannot be isolated from the upstream signal. For these reasons, the PM-NRZ scheme was accurately characterized in [11] using a specifically designed set-up that allowed a controlled generation of CB and SB. As described in [11] and [18], the two RB components were separately analyzed by modulating the signals at different points in order to reproduce the modulation characteristics of a PON. The upstream signal and the RB were generated in two separate arms of an interferometer allowing accurate control of OSRNR and polarization. For experimental convenience the OSRNR is defined at the point where the signals enter the wavelength multiplexer (Fig. 1), hence before the various signals are spectrally reshaped by the optical filters.

Fig. 8 shows the comparison between the measured penalties (symbols) and the penalties calculated using the model (lines) for both CB and SB, with optical filter offsets of 0 and 30 GHz in the case of PM-NRZ. The modeling results are in very good agreement with the experiments both for CB and SB and, for comparison, the figure also presents the penalties measured for NRZ modulation format. The agreement for low OSRNR, which corresponds to a high level of RB noise, is slightly worse in all cases, possibly due to small differences between the spectra and filter responses in the experiment and the idealized versions used in the model.

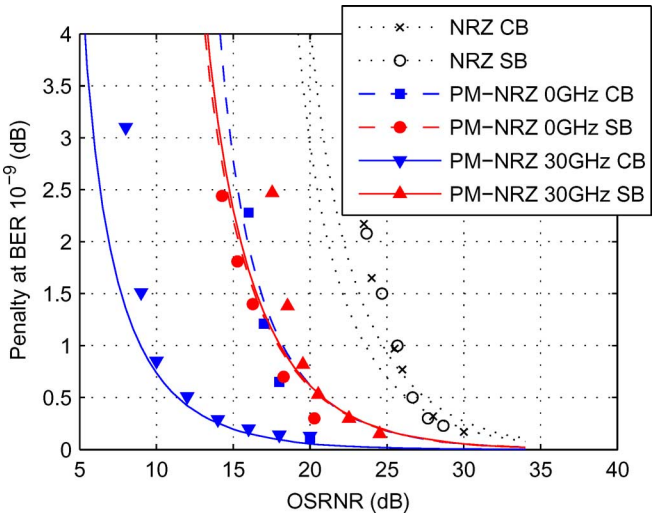

Fig. 8. Comparison between the measured (symbols) and modeled (lines) penalties as a function of OSRNR.

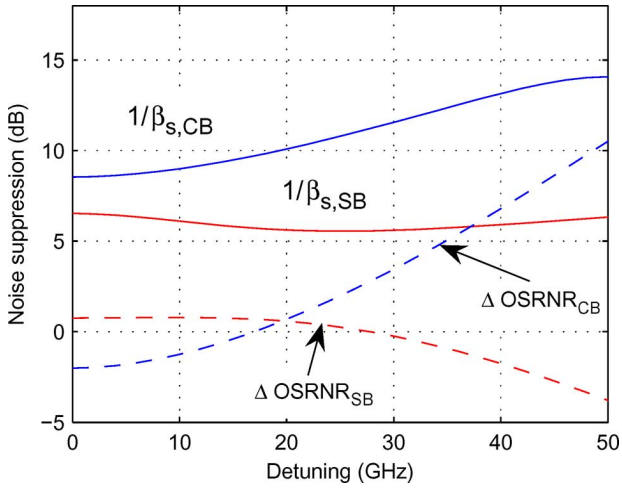

Fig. 9. Noise mitigation in CB and SB case introduced by the spectral broadening, $1/\beta_{s,x}$, and by the effective improvement of the OSRNR at the photodetector.

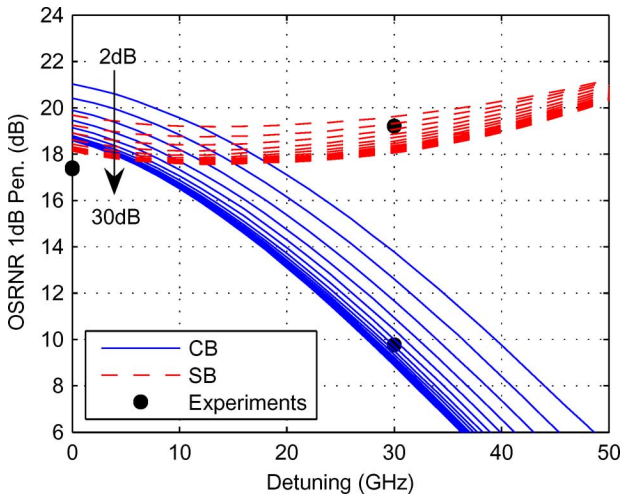

Fig. 10. Calculated (lines) and experimental (dots) OSRNR required for a 1-dB power penalty using the PM-NRZ modulation as a function of the filter detuning and for carrier suppression varying from 2 to 30 dB in 2-dB steps.

The performance of the scheme with respect to the SB is similar for the two detunings analyzed, due to the fact that the power spectrum of the SB is uniformly distributed over a range of frequencies larger than the AWG bandwidth (Fig. 4). As can be seen from Fig. 9, the noise reduction due to the spectral broadening, quantified by $1/\beta_{s,SB}$, is nearly constant for all detunings. However, as the detuning increases, the attenuation of the upstream signal, which is concentrated in the $\pm$10- and $\pm$20-GHz components, increases more rapidly than the SB, causing a relative increase in the noise. This effect is quantified by introducing the improvement in the OSRNR caused by the detuned filtering defined, in decibels, as the difference between the OSRNR at the receiver and the OSRNR before the wavelength multiplexer

$$\Delta\mathrm{OSRNR}_b = \mathrm{OSRNR}_{b,\mathrm{Rx}} - \mathrm{OSRNR}_b, \qquad (32)$$

with the subscript $_b$ indicating either CB or SB OSRNRs, which are in general affected in a different way due to their different spectra.

The opposite occurs in the CB case since the RB optical power is concentrated at the carrier frequency, which is attenuated by a greater amount than the signal as the detuning is increased, thus reducing the noise. This can also be clearly seen in Fig. 9, where both $1/\beta_{s,CB}$ and $\Delta\mathrm{OSRNR}_{\mathrm{CB}}$ further suppress the noise as the detuning increases. The spectral coefficient $1/\beta_{s,CB}$ increases because the attenuation of the component at the carrier frequency is relatively higher than the rest of the signal spectrum, reducing in this way the spectral overlap with the CB. The effective OSRNR at the photodetector simply increases due to the selective stronger filtering of the power at the carrier frequency, and hence of the CB, compared to the signal.

These two different behaviors of the PM-NRZ scheme as a function of the filter detuning for CB and SB are also clearly shown in Fig. 10, where the OSRNR required for a 1-dB penalty is plotted for CB and SB for various values of center frequency suppression, and with the dots representing the experimental points derived from Fig. 8. It is interesting to note that the improvement in the noise mitigation obtained by increasing the center wavelength suppression beyond 10 dB is relatively small. These results suggest that a suppression of 10 dB or less is already sufficient to obtain effective RB noise mitigation, indicating also that precise control of the phase modulation depth is not necessary.

These results confirm that the proposed model is particularly suited to study and optimize complex modulation schemes such as the PM-NRZ scheme. An earlier version of the model has already been used to simulate the effect of two common optical multiplexer filter shapes, Gaussian and flat-top, for two different channel spacings, 100 and 50 GHz, confirming the effectiveness of the approach [20]. Moreover, the model has also been recently used to analyze the performance of an alternative modulation format, known as carrier-suppressed-subcarrier amplitude-modulation phase shift keying (CSS-AMPSK), which can potentially provide better mitigation of the SB-induced noise and present a higher tolerance to chromatic dispersion [10].

VII. Conclusion

A model capable of studying the interferometric noise caused by RB on signals with an arbitrary modulation format has been derived for an optically preamplified receiver. Due to its simple realization and fast computation, the model enables efficient analysis of the performance of interferometric noise reduction techniques, which proves to be particularly useful to optimize the performance of complex schemes within practical systems. The model could also be readily extended to the case of an optically amplified link, such as the hybrid DWDM-TDM long reach PON in [12], or easily adapted to the simpler case of a nonoptically preamplifed receiver such as a PIN or an APD. The specific case of PM-NRZ modulation has been used as an example, demonstrating excellent agreement between modeling and experimental results. Various parameters of the PM-NRZ scheme have been analyzed in order to understand experimental results showing, for example, that precise control of the phase modulation is not necessary to obtain good noise suppression.

References

[1] H. Ueda, K. Okada, B. Ford, G. Mahony, S. Hornung, D. Faulkner, J. Abiven, S. Durel, R. Ballart, and J. Erickson, "Deployment status and common technical specifications for a B-PON system," *IEEE Commun. Mag.*, vol. 39, no. 12, pp. 134–141, Dec. 2001.

[2] R. Davey, J. Kani, F. Bourgart, and K. McCammon, "Options for future optical access networks," *IEEE Commun. Mag.*, vol. 44, no. 10, pp. 50–56, Oct. 2006.

[3] G. Talli and P. D. Townsend, "Hybrid DWDM-TDM long reach PON for next generation optical access," *J. Lightw. Technol.*, vol. 24, no. 7, pp. 2827–2834, Jul. 2006.

[4] K. Iwatsuki, J. Kani, H. Suzuki, and M. Fujiwara, "Access and metro networks based on WDM technologies," *J. Lightw. Technol.*, vol. 22, no. 11, pp. 2623–2630, Nov. 2004.

[5] E. K. MacHale, G. Talli, and P. D. Townsend, "10 Gb/s bidirectional transmission in a 116 km reach hybrid DWDM-TDM PON," in *Proc. Optical Fiber Communication Conf.*, 2006, p. OFE1.

[6] M. Fujiwara, J. Kani, H. Suzuki, and K. Iwatsuki, "Impact of backreflection on upstream transmission in WDM single-fiber loopback access networks," *J. Lightw. Technol.*, vol. 24, no. 2, pp. 740–746, Feb. 2006.

[7] R. K. Staubli and P. Gysel, "Crosstalk penalties due to coherent Rayleigh noise in bidirectional optical communication systems," *J. Lightw. Technol.*, vol. 9, no. 3, pp. 375–380, Mar. 1991.

[8] T. Yoshida, S. Kimura, H. Kimura, K. Kumozaki, and T. Imai, "A new single-fiber 10-Gb/s optical loopback method using phase modulation for WDM optical access networks," *J. Lightw. Technol.*, vol. 24, no. 2, pp. 786–796, Feb. 2006.

[9] Z. Li, Y. Dong, Y. Wang, and C. Lu, "A novel PSK-Manchester modulation format in 10-Gb/s passive optical network system with high tolerance to beat interference noise," *IEEE Photon. Technol. Lett.*, vol. 17, no. 5, pp. 1118–1120, May 2005.

[10] C. W. Chow, G. Talli, A. D. Ellis, and P. D. Townsend, "Rayleigh noise mitigation in DWDM LR-PONs using carrier suppressed subcarrier-amplitude modulated phase shift keying," *Opt. Exp.*, vol. 16, pp. 1860–1866, January 2008.

[11] C. W. Chow, G. Talli, and P. D. Townsend, "Rayleigh noise reduction in 10-Gb/s DWDM-PONs by wavelength detuning and phase-modulation-induced spectral broadening," *IEEE Photon. Technol. Lett.*, vol. 19, no. 3, pp. 423–425, Mar. 2007.

[12] G. Talli, C. W. Chow, E. K. MacHale, and P. D. Townsend, "Rayleigh noise mitigation in long reach hybrid DWDM-TDM PONs," *J. Opt. Netw.*, vol. 6, pp. 765–776, Jun. 2007.

[13] N. Olsson, "Lightwave systems with optical amplifiers," *J. Lightw. Technol.*, vol. 7, no. 7, pp. 1071–1082, Jul. 1989.

[14] R. C. Steele, G. R. Walker, and N. G. Walker, "Sensitivity of optically preamplified receivers with optical filtering," *IEEE Photon. Technol. Lett.*, vol. 3, no. 6, pp. 545–547, Jun. 1991.

[15] P. J. Winzer, M. Pfennigbauer, M. M. Strasser, and W. R. Leeb, "Optimum filter bandwidths for optically preamplified NRZ receivers," *J. Lightw. Technol.*, vol. 19, no. 9, pp. 1263–1273, Sep. 2001.

[16] J. L. Rebola and A. V. T. Cartaxo, "Gaussian approach for performance evaluation of optically preamplified receivers with arbitrary optical and electrical filters," *IEE Proc. Optoelectron.*, vol. 148, pp. 135–142, Jun. 2001.

[17] I. T. Lima, Jr., A. O. Lima, Y. Sun, H. Jiao, J. Zweck, C. R. Menyuk, and G. M. Carter, "A receiver model for optical fiber communication systems with arbitrarily polarized noise," *J. Lightw. Technol.*, vol. 23, no. 3, pp. 1478–1490, Mar. 2005.

[18] G. Talli, D. Cotter, and P. D. Townsend, "Rayleigh backscattering impairments in access networks with centralised light source," *Electron. Lett.*, vol. 42, pp. 877–878, Jul. 2006.

[19] J. L. Rebola and A. V. T. Cartaxo, "Q-factor estimation and impact of spontaneous-spontaneous beat noise on the performance of optically preamplified systems with arbitrary optical filtering," *J. Lightw. Technol.*, vol. 21, no. 1, pp. 87–95, Jan. 2003.

[20] G. Talli, C. W. Chow, and P. D. Townsend, "Filter impact in spectrally-broadened Rayleigh noise reduction schemes for DWDM-PONs," in *Proc. Optical Fiber Communication Conf.*, 2007, p. OWD4.

Giuseppe Talli (S'01–M'03) received the Laurea degree in electronic engineering from the University of Padova, Padova, Italy, in 2000, and the Ph.D. degree in electronic engineering from the University of Essex, Essex, U.K., in 2003, for work on the effects of the amplified spontaneous emission in semiconductor optical amplifiers and their gain dynamics.

Since 2004, he has been with the Tyndall National Institute and the Department of Physics, University College Cork, Ireland, where he is a Staff Research Scientist in the Photonic Systems Group working in the area of optical access networks.

Chi Wai Chow (M'04) received the B.Eng. (first class hons) and Ph.D. degrees from the Department of Electronic Engineering, Chinese University of Hong Kong, in 2001 and 2004, respectively.

After graduation, he was appointed as a Postdoctoral Fellow at the Chinese University of Hong Kong, working on optical packet switched networks and silicon photonics. Between 2005–2007, he was with the Photonic Systems Group, Tyndall National Institute and University College Cork, Ireland, working as a Postdoctoral Research Scientist in the area of optical access networks. In August 2007, he joined the Department of Photonics, National Chiao Tung University, Taiwan, R.O.C., as an Assistant Professor.

Paul D. Townsend (M'04) received the B.Sc. degree in physics from the University of East Anglia, Norwich, U.K., in 1983, and the PhD. degree in physics from the University of Cambridge, Cambridge, U.K., in 1987.

From 1987 to 1990, he held a joint position with St. John's College, Cambridge, and with Bellcore, Red Bank, NJ, and in 1990, he joined British Telecom Laboratories, Ipswich, U.K., where he worked on various aspects of quantum optics and optical communications including quantum cryptography. In 2000, he joined the Corning Research Centre, Ipswich, where he was a Project Manager for access network applications research. Since 2003, he has been with the Tyndall National Institute and the Department of Physics, University College Cork, Ireland, where he leads the access networks and quantum communications research activities in the Photonic Systems Group.

He is a Fellow of the Institute of Physics (U.K.) and an Honorary Professor in the School of Engineering and Physical Sciences, Heriot-Watt University, Edinburgh, U.K.